A Study of Lattice Expansion in CeO_2 Nanoparticles by Transmission Electron Microscopy

R. K. Hailstone,*,† A. G. DiFrancesco,† J. G. Leong,‡ T. D. Allston,‡ and K. J. Reed§

Center for Imaging Science, Rochester Institute of Technology, Rochester, New York 14623, Department of Chemistry, Rochester Institute of Technology, Rochester, New York 14623, and Cerion Energy Corporation, One Blossom Road, Rochester, New York 14610

Received: April 15, 2009; Revised Manuscript Received: July 7, 2009

Nanoceria was produced by an aqueous precipitation technique in the presence of an organic stabilizer. The stable suspensions were diafiltered to remove reaction byproducts. Particles were characterized by transmission electron microscopy with images used to size the particles, and selected-area electron diffraction was used to determine the lattice structure and the lattice constant. For all particles studied, the electron diffraction data were consistent with that of CeO_2 and not Ce_2O_3, as predicted by some researchers for very small particles sizes. At particle diameters of ~1 nm, the lattice expansion approached 7%. In agreement with earlier researchers, we interpret this effect as due to the formation of substantial amounts of Ce^{3+} with corresponding oxygen vacancies, but within the fluorite lattice structure of CeO_2. Even at a particle size of 1 nm, there was a measurable oxygen storage capacity, consistent with a still-reducible CeO_2 structure, rather than the fully oxidized Ce_2O_3.

Introduction

Nanocrystalline CeO_2 (nanoceria) has many real and potential applications.[1] It is an important component in three-way automotive catalysts[2] and is used in solid oxide fuel cells.[3] Its reactivity is connected to its redox chemistry, involving the facile Ce^{4+}/Ce^{3+} electrochemistry.[1] This allows nanoceria to store oxygen under oxidizing conditions (Ce^{4+}) and to release oxygen under reducing conditions (O vacancies are created, leading to the formation of Ce^{3+}).

Many techniques for synthesis have been used to produce nanoceria, such as chemical precipitation,[4] hydrothermal,[5] alchothermal,[6] and thermal evaporation.[7] Most wet methods produce an unstable suspension of the nanoparticles, leading to agglomeration. For some potential applications, it would be desirable to produce a thermodynamically stable colloidal suspension. We have devised such a process based on aqueous precipitation in the presence of an organic stabilizer in which particles with diameters of 1−4 nm form a stable suspension.[8] Reaction byproducts can be removed by diafiltration, after which the particles can be shifted into a nonaqueous solvent by dialysis and further drying over molecular sieves.

Of primary concern in the present study is the composition of our particles at very small sizes. Because of the ease of O removal and addition, the formula for ceria is often written as CeO_{2-x}, where x ranges from 0 to 0.5, depending on conditions of preparation and treatment of the nanoparticles. Earlier work by Tsunekawa and co-workers suggested that $x = 0.5$ for particles with ~1.5 nm diameters and smaller and that the lattice was that of the cubic form of Ce_2O_3 (C-type), the fully reduced form of ceria.[9] Subsequent work, involving X-ray photoelectron spectroscopy (XPS), lead to the conclusion that the increase in the lattice constant at small particle sizes was due to the increased surface-to-volume ratio and that the surface was largely Ce^{3+}.[10] The latter observation is consistent with those of several other studies.[11]

These experimental studies were supported by theoretical studies of Skorodumova and co-workers using a density functional theory (DFT) approach incorporating the full-potential linear muffin orbitals (FP-LMTO) method.[12] They concluded that the delocalization−localization of the Ce 4f electrons is involved in the $CeO_2-Ce_2O_3$ transition. The C-type structure of Ce_2O_3 can be constructed out of eight unit cells of CeO_2 with 25% O vacancies ordered in a particular way. Minimal reorganization of the basic lattice is required, making the oxidation−reduction process facile. Following reduction, the added electron is localized on the Ce core (4f orbital), as opposed to a delocalized valence electron in CeO_2, which results in a 10% volume increase.

A value of $x = 0.5$ was later confirmed by Wu and co-workers for particles with ~3 nm diameters, but their electron diffraction data were consistent with the fluorite lattice expected for CeO_2.[7] On the basis of the results of electron energy loss spectroscopy (EELS), they concluded that, at ~3 nm, the ceria lattice consisted solely of Ce^{3+}. In other words, the nanoparticles were completely reduced. Such particles should have zero oxygen storage capacity (OSC). Wu and co-workers also modeled their particles as having a core−shell structure in which the core was CeO_2 and the shell $CeO_{1.5}$. Although they acknowledged that this was an approximation, it captured the essence of their hypothesis that the outer part of their particles was highly depleted of O and, therefore, largely Ce^{3+}.

In a theoretical study using DFT augmented by the use of the Hubbard Hamiltonian and providing for the localization of strongly correlated electrons, Loschen and co-workers studied a series of $(CeO_{2-x})_n$ clusters up to $Ce_{85}O_{160}$.[13] This latter cluster size would correspond to an ~2 nm diameter. Lattice expansion was found as the cluster size decreased, and this was attributed to increasing amounts of Ce^{3+} at the surface of the smaller clusters, which would lead to reduced Ce−O electrostatic attraction. However, increased numbers of Ce^{3+} alone would not fully account for the observed lattice expansion. These

* Corresponding author. E-mail: hailstone@cis.rit.edu.
† Center for Imaging Science, Rochester Institute of Technology.
‡ Department of Chemistry, Rochester Institute of Technology.
§ Cerion Energy Corporation.

10.1021/jp903468m CCC: $40.75
Published on Web 07/31/2009

authors concluded that O vacancies are also necessary to account for the lattice expansion. In addition, they also suggested that there would be a range of interatomic distances in the vacancy-ladened small clusters, making the concept of a single lattice constant somewhat dubious.

More recently, lattice expansion was again observed for small (down to 3 nm diameter) CeO_2 nanoparticles by Deshpande and co-workers.[14] On the basis of their XPS data, they conclude that the fraction of Ce ions in the +3 state increases as the particle size decreases and this is attributed to a higher O vacancy concentration. Furthermore, higher Ce^{3+} concentration leads to higher lattice strain and the observed increase in the lattice constant at a 3 nm particle diameter.

In the present work, we have studied particles as small as 1.1 nm mean diameter and have found no evidence of a cubic Ce_2O_3 lattice. Remarkably, at this size, the electron diffraction data indicate the fluorite lattice of CeO_2. Because of the relatively large increase in the lattice constant at this small size, the particles are characterized by substantial amounts of Ce^{3+} and corresponding O vacancies.

Experimental Methods

Aqueous solutions of organic stabilizer and $Ce(NO_3)_3 \cdot 6H_2O$ were added to a water-jacketed reaction vessel. Next, a 50% H_2O_2 solution was added and the vessel was mixed with a high-speed shearing mixer at 8100 rpm. Aqueous 28−30% NH_4OH was added under high-speed mixing, after which a prop stirrer was used at 500 rpm. The reactor temperature was raised to 70 °C over 30 min and then held at 70 °C for 50−90 min, depending on the particular formulation. The reaction vessel was cooled to room temperature over 30 min and then diafiltered with a Millipore 3 kDa ultrafiltration membrane to an ionic conductivity of 3 mS/cm^2 or less.

Particle formation appears to proceed through a $Ce(OH)_3$ intermediate phase, followed by oxidation to CeO_2 by H_2O_2, probably in the form of OH radicals. For 1.1 nm particles, a stabilizer combination of ethylenediaminetetraacetic acid and lactic acid was used, whereas 2 nm particles were stabilized by methoxyethoxyethoxyacetic acid. The largest particles studied (11.8 nm) were prepared by the method of Chen and Chang.[4] In this case, no stabilizer was used and the particles were not diafiltered. The latter is not colloidally stable, but it does provide an experimental point between bulk ceria and our colloidally stable nanoparticles.

Specimens for TEM examination were prepared from the diafiltered aqueous suspension by a suitable dilution in 0.02 M solution of an organic stabilizer. A 10 μL drop of the diluted suspension was placed on a carbon-film-covered copper grid and allowed to air dry. Images and selected-area diffraction patterns were obtained in either a JEOL 2000FX or a 100CX TEM, both with tungsten filaments. Image magnification was calibrated using phase-contrast images of asbestos fibers. High-resolution (HRTEM) images were obtained on a JEOL 2010F TEM. Images were recorded on Kodak 4489 electron microscope film and digitized with a Nikon 9000 film scanner.

Particle sizing was done with Image J. First, the images were histogram-equalized to improve their contrast. Then, they were thresholded to give a binary image with the threshold adjusted to give the same particle size as in the original image. Next, areas were determined for 100−200 particles and, from these, the number-averaged diameter was calculated, assuming spherical morphology. For electron diffraction, the camera length was calibrated using a TlCl microcrystal standard. The radii of diffraction rings were determined using the radial profile plug-in in Image J.

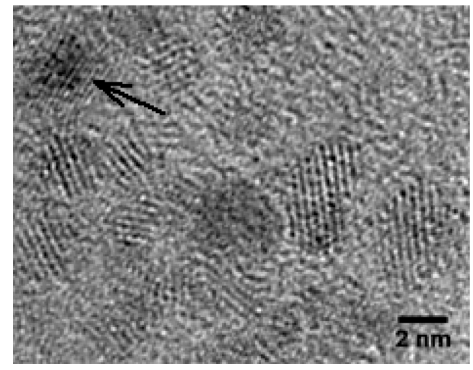

Figure 1. HRTEM image of 2 nm CeO_2 nanoparticles. The arrow indicates a difference from the rest of the nanoparticles (see text).

Oxygen storage capacity was measured using a TA Instruments Q500 thermogravimetric analyzer (TGA). A 50−90 mg sample of CeO_2 was heated in the TGA furnace to 700 °C under air and allowed to stay at that temperature for 15 min. The sample was exposed to a reducing environment consisting of 5% H_2 in nitrogen for 40 min. Then, the sample was exposed to air for 15 min. This was all completed at 700 °C. The weight change was recorded by the TA Instruments TGA. The calculation used is (final weight under oxygen − final weight under H_2/N_2)/(32 × sample weight), and the measured values are reported as μmol of O_2/g of CeO_2. The theoretical maximum value is 1454 μmol of O_2/g of CeO_2. The 2 σ confidence interval in the measured values is ∼10%, based on three replicates. Cerium oxide powder was obtained from Sigma-Aldrich and used without further purification. This material was used as a "bulk" reference for OSC measurements.

Results

Figure 1 shows a HRTEM image of 2 nm CeO_2 nanoparticles and demonstrates the single-crystalline nature of our material. This image and other similar fields show that the particles are mainly bounded by (111) planes. This is expected for CeO_2 because the (111) plane is considered to be the most stable.[17,18] However, there are a few particles that are bounded by (220) planes (arrow in the image). This image corresponds to the lower-magnification image in Figure 2C and is representative of images from other fields of this sample.

Figure 2 shows the images and selected-area diffraction patterns for four different nanoparticle suspensions. The mean number-averaged diameter and lattice constant obtained from the electron diffraction data are given in Table 1. The diffraction pattern for all nanoparticles is consistent with that of the fluorite lattice structure of CeO_2 and not with the structure expected for Ce_2O_3, either the cubic or the hexagonal form. In particular, the most intense line expected for C-type Ce_2O_3 is the (511) line corresponding to 0.2184 nm lattice spacing, whereas, experimentally, our most intense line is the (111) corresponding to 0.312 nm lattice spacing, as expected for the fluorite structure of CeO_2.

It is well-known that both X-ray and electron diffraction lines broaden in powder diffraction patterns as the crystallite size decreases.[19] In fact, the half width at half-maximum is inversely proportional to the crystallite diameter to the first power. This behavior is evident in our electron diffraction data by comparing Figure 2A through C to D. Therefore, it was of concern that error is introduced to our lattice constant measurement because

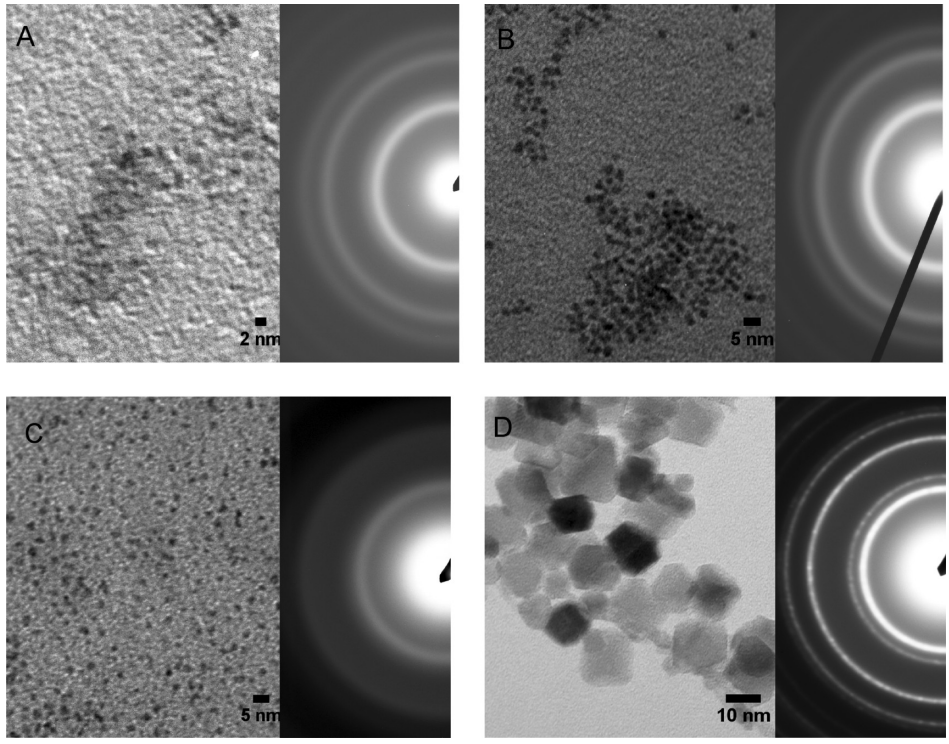

Figure 2. TEM images and electron diffraction patterns for four nanoparticle preparations: (A) 1.1 nm diameter, (B) 2 nm diameter, (C) 2 nm diameter (showing reproducibility), and (D) 11.8 nm diameter.

TABLE 1: Mean Diameter, Lattice Constant, and % Lattice Expansion

mean diameter, nm	lattice constant,[a] nm	% lattice expansion	OSC,[c] μmol of O_2/g of CeO_2
1.1 ± 0.3	0.578	6.8	65
2.0 ± 0.5	0.555	2.6	349
2.0 ± 0.5	0.555	2.6	
11.8 ± 1.2	0.547	1.1	425
bulk	0.541[b]		296

[a] Calculated from d_{111} spacing using $a = d_{111}\sqrt{(h^2 + k^2 + l^2)} = d_{111}\sqrt{3}$. The 2 σ uncertainty is ± 0.006. [b] See ref 1, p 15. [c] The 2 σ uncertainty is $\pm 10\%$.

of the diffuseness of the rings. To check this, we acquired electron diffraction patterns for the 1.1 nm diameter nanoparticles at five different regions on the grid. When the inner, most-intense ring is used, the measured lattice spacing had a 1 σ deviation of 0.003 nm or a coefficient of variation of less than 1%.

A plot of lattice constant versus particle diameter and the degree of lattice expansion versus particle diameter are shown in Figure 3. The expansion of the lattice plotted in Figure 3A follows the empirical equation

$$a = a_{\text{bulk}} + 0.036/D$$

where a is the lattice constant of the nanoparticle suspension, a_{bulk} is the lattice constant of bulk CeO_2, and D is the particle mean diameter. Figure 3B shows that the lattice expansion approaches 7% at approximately a 1 nm diameter, yet Figure 2A shows that the fluorite lattice persists even at this small size.

Following previous work discussed above, we would expect the large lattice expansion observed for our smallest nanoparticle to be largely due to a significant number of Ce^{3+} and corresponding O vacancies. However, it is well-known that, in an

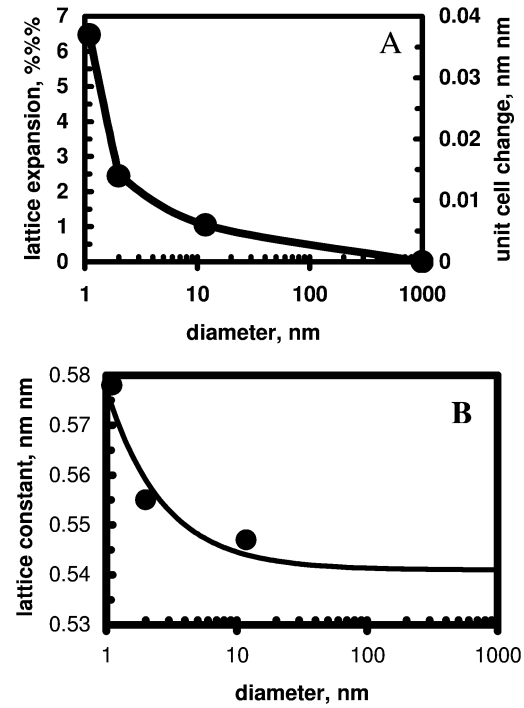

Figure 3. (A) Lattice constant vs particle mean diameter. The curve is defined by the equation given in the text. (B) Lattice expansion vs particle mean diameter.

electron beam, reduction of Ce^{4+} to Ce^{3+} can occur in CeO_2.[15] This reduction is more likely to occur with a high brightness field emission gun than with our tungsten-based gun, particularly with a largely expanded beam used for imaging electron diffraction patterns. We tested for this possibility anyway by, first, imaging a diffraction pattern of our smallest particle in one area of the specimen, then translating to a previously unexposed area and rapidly acquiring another diffraction pattern

without going back to normal imaging mode. Within experimental error, we could detect no difference in the lattice constant derived from these two diffraction patterns.

Oxygen storage capacity data are summarized in Table 1 and show that the measured OSC tends to increase as particle size decreases and then decreases as particle size decreases further. Most importantly, however, there is a residual OSC at the smallest particle size.

Discussion

Our results extend those of other researchers to smaller particle sizes. Wu and co-workers studied particles as small as 3 nm in diameter, finding no evidence for the C-type Ce_2O_3.[7] But the work of Tsunekawa and co-workers suggests that, at this size, we should not expect to see Ce_2O_3; rather, it should be observed at ~1.5 nm and smaller.[9] We have now extended the size range down to ~1 nm but still find no evidence of the cubic form of Ce_2O_3. Because of our smaller particle size compared with all known previous work, our lattice expansion of almost 7% is the highest seen for nanoceria.

The lattice expansion observed by us and others for CeO_2 is quite different from that observed for other materials. Recently, Zuo and co-workers have used coherent electron nanodiffraction to obtain electron diffraction patterns for single nanocrystals. Their data show that the first one or two atomic layers contract inward in both gold and CdSe nanocrystals.[16] Computer simulations of (111) ideal (no vacancies) CeO_2 layers, which we expect to be the most stable surfaces for our synthesis conditions based on both theoretical calculations[17] and experimental measurements,[18] showed that anion-terminated surfaces had a slight (0.16%) contraction.[17] The anion-terminated surfaces were suggested to be dominant. The very low contraction was suggested to be due to low strain on the (111) surface where anions and cations are in separate planes. However, no account of the possible presence of Ce^{3+} and associated vacancies was studied in this work.

It is interesting to compare our measured lattice expansion with that predicted by others at a 1 nm particle diameter. Because there is not a linear relationship between lattice parameter and particle diameter and because, in some cases, there are only a few data points, the extrapolation to smaller diameter is very crude. Nevertheless, lattice expansions between 4.3 and 6.3% are expected at ~1 nm based on the work reported in refs 7, 9, and 14. This compares favorably with our measured value of 6.8%.

When we use a simple cubic lattice model for our particles, at ~1 nm, the particle consists of eight unit cells in which ~80% of the cerium ions is at the surface of the particle. In agreement with many earlier studies, we suggest that the vast majority of these surface ions is Ce^{3+} and there is a corresponding large number of oxygen vacancies (one for each pair of Ce^{3+} formed). The larger radius of Ce^{3+} versus Ce^{4+}, along with the associated O vacancies, would explain the larger lattice constant observed at small sizes. Likewise, the resulting lattice strain leads to the observed lattice expansion. Our lattice constant data are approximately consistent with an empirical equation, and this equation is consistent with similar versions found in the literature.[13,14]

Oxygen storage capacity is further support for the proposed mechanism of lattice expansion. Intuitively, one would expect that the OSC would increase with smaller particle size because of increased surface area/mole. However, this is counteracted by the tendency to form Ce^{3+} at the surface of CeO_2 particles,[13,14] which introduces O vacancies. These O vacancies are known to be more stable at the surface than in the bulk,[20] which impedes O diffusion to the surface and lowers the expected OSC.

Our experimental data are at least qualitatively consistent with this expected trend. The OSC increases in going from bulk powder (micrometer sized crystallites) to 11.8 nm nanoparticles. However, a further decrease in size to 2 nm causes the OSC to decrease as the O vacancies associated with the surface Ce^{3+} become an important factor in controlling OSC. A further decrease in particle size to 1.1 nm leads to 80% of the Ce ions in the particle being Ce^{3+}. The increase in O vacancies causes the OSC to dramatically decrease. However, the more than 5-fold decrease in OSC relative to the 2 nm particle is more than expected based on simple arguments regarding numbers of Ce^{3+} and O vacancies, suggesting our understanding of the processes controlling OSC at these very small particle sizes is incomplete.

These OSC data indicate that, at an ~1 nm diameter, there is some small oxygen storage capacity. This result conflicts with the proposal of Wu and co-workers who suggest that, based on their EELS data, below ~3 nm, the particle should be composed completely of Ce^{3+}, that is, Ce_2O_3, but with the fluorite lattice structure. Perhaps this discrepancy is due to the quite different modes of particle synthesis used in our work (aqueous-based) versus that of Wu and co-workers (thermal evaporation). Alternatively, perhaps their experimental conditions did not completely eliminate reduction by the electron beam. Additionally, our OSC results provide an explanation for why the fluorite lattice structure persists at a 1 nm diameter. Evidence of an oxygen storage capacity at this particle size indicates that there are Ce^{4+} ions present in the particle, which would require the fluorite lattice structure.

Conclusions

Colloidally stable CeO_2 nanoparticles can be prepared by aqueous precipitation techniques using suitable organic stabilizers. The particles are highly crystalline with predominantly (111) surfaces. Selected-area electron diffraction data indicate that the fluorite lattice structure persists for particle sizes as small as 1 nm. Oxygen storage capacity measurements indicate that Ce^{4+} ions are present at 1 nm size, consistent with a fluorite lattice. At this size, the particles have substantial amounts of Ce^{3+} that, together with the associated O vacancies, lead to large lattice strain and a lattice expansion of almost 7%.

Acknowledgment. The financial support of Cerion Energy Corporation is gratefully appreciated. HRTEM images were provided by M. Rodriguez, the University at Albany, State University of New York.

References and Notes

(1) Trovarelli, A. *Catalysis by Ceria and Related Materials*; Trovarelli, A., Ed.; Imperial College Press: London, 2002; Chapter 2.

(2) Nunan, J.; Robota, H. J.; Cohn, M. J.; Bradley, S. A. *J. Catal.* **1992**, *133*, 309–324.

(3) Mo, L.; Zheng, X.; Yeh, C.-T. *Chem. Commun.* **2004**, 1426–1427.

(4) (a) Chen, H.-I.; Chang, H.-Y. *Ceram. Int.* **2005**, *31*, 795–802. (b) Zhang, F.; Jin, Q.; Chan, S.-W. *J. Appl. Phys.* **2004**, *95*, 4319–4326.

(5) (a) Hirano, M.; Inagaki, M. *J. Mater. Chem.* **2000**, *10*, 473–477. (b) Hirano, M.; Kato, E. *J. Am. Ceram. Soc.* **1996**, *79*, 777–780. (c) Masui, T.; Hirai, H.; Imanaka, N.; Adachi, G. *J. Mater. Sci. Lett.* **2002**, *21*, 489–491. (d) Kaneko, K.; Inoke, K.; Freitag, B.; Hungria, A. B.; Midgley, P. A.; Hansen, T. W.; Zhang, J.; Ohara, S.; Adschhiri, T. *Nano Lett.* **2007**, *7*, 421–425.

(6) Zhang, Y.-W.; Si, R.; Liao, C.-S.; Yan, C.-H.; Xiao, C.-X.; Kou, Y. *J. Phys. Chem. B* **2003**, *107*, 10159–10167. Si, R.; Zhang, Y.-W.; You, L. P.; Yan, C. R. *J. Phys. Chem. B* **2006**, *110*, 5994–6000.

(7) Wu, L.; Wiesmann, H.; Moodenbaugh, A.; Klie, R.; Zhu, Y.; Welch, D.; Suenaga, M. *Phys. Rev. B* **2004**, *69*, 125415-1–125415-9.

(8) DiFrancesco, A. G.; Hailstone, R. K.; Langner, A.; Reed, K. J. U. S. Patent Application PCT/US07/77545.

(9) Tsunekawa, S.; Sivamohan, R.; Ito, S.; Kasuya, A.; Fukuda, T. *Nanostruct. Mater.* **1999**, *11*, 141–147.

(10) (a) Tsunekawa, S.; Sahara, R.; Kawazoe, Y.; Ishikawa, K. *Appl. Surf. Sci.* **1999**, *152*, 53–56. (b) Tsunekawa, S.; Ishikawa, K.; Li, Z.-Q.; Kawazoe, Y.; Kasuya, A. *Phys. Rev. Lett.* **2000**, *85*, 3440–3443. (c) Tsunekawa, S.; Fukuda, T.; Kasuya, A. *Surf. Sci.* **2000**, *457*, L437–L440.

(11) (a) Sharma, R.; Crozier, P. *Microsc. Microanal.* **2002**, *8*, 600CD−601CD, Supplement S02. (b) Wu, L.; Wiesmann, H. J.; Moodenbaugh, A. R.; Fischer, D. A.; Zhu, Y.; Suenga, M. *Microsc. Microanal.* **2003**, *9*, 820−821, Supplement S02. (c) Gilliss, S. R.; Bentley, J.; Carter, C. B. *Microsc. Microanal.* **2003**, *9*, 420−421, Supplement S02. (d) Gilliss, S. R.; Bentley, J.; Carter, C. B. *Mater. Res. Soc. Symp. Proc.* **2004**, *818*, M1.8.1−M1.8.6. (e) Sharma, R.; Crozier, P.; Kang, Z. C.; Eyring, L. *Philos. Mag.* **2004**, *84*, 2731–2747. (f) Gilliss, S. R.; Bentley, J.; Carter, C. B. *Appl. Surf. Sci.* **2005**, *241*, 61–67. (g) Wang, R.; Crozier, P. A.; Sharma, R.; Adams, J. B. *Nano Lett.* **2008**, *8*, 962–967.

(12) (a) Skorodumva, N. V.; Ahuja, R.; Simak, S. I.; Abrikosov, I. A.; Johansson, B.; Lundqvist, B. I. *Phys. Rev. B* **2001**, *64*, 115108-1–115108-9. (b) Skorodumva, N. V.; Simak, S. I.; Lundqvist, B. I.; Abrikosov, I. A.; Johansson, B. *Phys. Rev. Lett.* **2002**, *89*, 166601-1–166601-4.

(13) Loschen, C.; Bromley, S. T.; Neyman, K. M.; Illas, F. *J. Phys. Chem. C* **2007**, *111*, 10142–10145.

(14) Deshpande, S.; Patil, S.; Kuchibhatla, S. V. N. T.; Seal, S. *Appl. Phys. Lett.* **2005**, *87*, 133113-1–133113-3.

(15) Garvie, L. A. J.; Buseck, P. R. *J. Phys. Chem. Solids* **1999**, *60*, 1943–1947.

(16) Huang, W. J.; Sun, R.; Tao, J.; Menard, L. D.; Nuzzo, R. G.; Zuo, J. M. *Nat. Mater.* **2008**, *7*, 308–313. Huang, W. J.; Zuo, J. M.; Jiang, B.; Kwon, K. W.; Moonsub, S. *Nat. Phys.* **2009**, *5*, 129–133.

(17) Sayle, T. X. T.; Parker, S. C.; Catlow, C. R. A. *Surf. Sci.* **1994**, *316*, 329–336.

(18) Wang, Z. L.; Feng, X. *J. Phys. Chem. B* **2003**, *107*, 13563–13566. Barnard, A. S.; Kirkland, A. I. *Chem. Mater.* **2008**, *20*, 5460–5463.

(19) Fultz, B.; Howe, J. *Transmission Electron Microscopy and Diffractometry of Materials*, 3rd ed.; Springer: New York, 2008; Chapter 8.

(20) Trovarelli, A. *Catalysis by Ceria and Related Materials*; Trovarelli, A., Ed.; Imperial College Press: London, 2002; p 319.

JP903468M